

NASA/TM—2002-211495



# Performance Validation Approach for the GTX Air-Breathing Launch Vehicle

Charles J. Trefny and Joseph M. Roche  
Glenn Research Center, Cleveland, Ohio

---

April 2002

## The NASA STI Program Office . . . in Profile

Since its founding, NASA has been dedicated to the advancement of aeronautics and space science. The NASA Scientific and Technical Information (STI) Program Office plays a key part in helping NASA maintain this important role.

The NASA STI Program Office is operated by Langley Research Center, the Lead Center for NASA's scientific and technical information. The NASA STI Program Office provides access to the NASA STI Database, the largest collection of aeronautical and space science STI in the world. The Program Office is also NASA's institutional mechanism for disseminating the results of its research and development activities. These results are published by NASA in the NASA STI Report Series, which includes the following report types:

- **TECHNICAL PUBLICATION.** Reports of completed research or a major significant phase of research that present the results of NASA programs and include extensive data or theoretical analysis. Includes compilations of significant scientific and technical data and information deemed to be of continuing reference value. NASA's counterpart of peer-reviewed formal professional papers but has less stringent limitations on manuscript length and extent of graphic presentations.
- **TECHNICAL MEMORANDUM.** Scientific and technical findings that are preliminary or of specialized interest, e.g., quick release reports, working papers, and bibliographies that contain minimal annotation. Does not contain extensive analysis.
- **CONTRACTOR REPORT.** Scientific and technical findings by NASA-sponsored contractors and grantees.

- **CONFERENCE PUBLICATION.** Collected papers from scientific and technical conferences, symposia, seminars, or other meetings sponsored or cosponsored by NASA.
- **SPECIAL PUBLICATION.** Scientific, technical, or historical information from NASA programs, projects, and missions, often concerned with subjects having substantial public interest.
- **TECHNICAL TRANSLATION.** English-language translations of foreign scientific and technical material pertinent to NASA's mission.

Specialized services that complement the STI Program Office's diverse offerings include creating custom thesauri, building customized data bases, organizing and publishing research results . . . even providing videos.

For more information about the NASA STI Program Office, see the following:

- Access the NASA STI Program Home Page at <http://www.sti.nasa.gov>
- E-mail your question via the Internet to [help@sti.nasa.gov](mailto:help@sti.nasa.gov)
- Fax your question to the NASA Access Help Desk at 301-621-0134
- Telephone the NASA Access Help Desk at 301-621-0390
- Write to:  
NASA Access Help Desk  
NASA Center for Aerospace Information  
7121 Standard Drive  
Hanover, MD 21076

NASA/TM—2002-211495



# Performance Validation Approach for the GTX Air-Breathing Launch Vehicle

Charles J. Trefny and Joseph M. Roche  
Glenn Research Center, Cleveland, Ohio

Prepared for the  
Combustion, Airbreathing Propulsion, Propulsion Systems Hazards, and  
Modelling and Simulation Subcommittees Joint Meeting  
sponsored by the Joint Army-Navy-NASA-Air Force  
Destin, Florida, April 8–12, 2002

National Aeronautics and  
Space Administration

Glenn Research Center

---

April 2002

Trade names or manufacturers' names are used in this report for identification only. This usage does not constitute an official endorsement, either expressed or implied, by the National Aeronautics and Space Administration.

Available from

NASA Center for Aerospace Information  
7121 Standard Drive  
Hanover, MD 21076

National Technical Information Service  
5285 Port Royal Road  
Springfield, VA 22100

Available electronically at <http://gltrs.grc.nasa.gov/GLTRS>

# PERFORMANCE VALIDATION APPROACH FOR THE GTX AIR-BREATHING LAUNCH VEHICLE

Charles J. Trefny and Joseph M. Roche  
National Aeronautics and Space Administration  
Glenn Research Center  
Cleveland, Ohio 44135

## ABSTRACT

The primary objective of the GTX effort is to determine whether or not air-breathing propulsion can enable a launch vehicle to achieve orbit in a single stage. Structural weight, vehicle aerodynamics, and propulsion performance must be accurately known over the entire flight trajectory in order to make a credible assessment. Structural, aerodynamic, and propulsion parameters are strongly interdependent, which necessitates a system approach to design, evaluation, and optimization of a single-stage-to-orbit concept. The GTX reference vehicle serves this purpose, by allowing design, development, and validation of components and subsystems in a system context. The reference vehicle configuration (including propulsion) was carefully chosen so as to provide high potential for structural and volumetric efficiency, and to allow the high specific impulse of air-breathing propulsion cycles to be exploited. Minor evolution of the configuration has occurred as analytical and experimental results have become available. With this development process comes increasing validation of the weight and performance levels used in system performance determination. This paper presents an overview of the GTX reference vehicle and the approach to its performance validation. Subscale test rigs and numerical studies used to develop and validate component performance levels and unit structural weights are outlined. The sensitivity of the equivalent, effective specific impulse to key propulsion component efficiencies is presented. The role of flight demonstration in development and validation is discussed.

## SUMMARY

The primary objective of the GTX effort is to determine whether or not air-breathing propulsion can enable a reusable, single-stage-to-orbit launch vehicle. The program is based on maturation of a reference vehicle configuration with good potential for simplicity and structural efficiency. Demonstration of equivalent, effective specific impulse ( $I^*$ ) equal to 500 seconds and a 20% dry weight fraction is the program goal. Levels of component, propulsion system, and structural efficiency required to meet this goal have been determined. A comprehensive series of test rigs is being used to develop components, validate efficiency levels, and verify material properties. Once complete, these results will represent validation of the reference vehicle concept to Technology Readiness Level (TRL) 3-4. Subsequent ground demonstration of a flight-weight propulsion system along with large-scale structural verification increases the TRL to 5-6. A subscale, suborbital flight demonstration is proposed for validation to TRL 7 and to provide installed performance information at scale and conditions not available in ground test facilities.

## INTRODUCTION

Of the technical factors that would contribute to lowering the cost of space access, reusability has high potential. A fully reusable system would achieve orbit in a single stage and require little maintenance between flights. For a vehicle powered by chemical rockets, roughly 90% of the vehicle's gross lift-off weight (GLOW) is accounted for by the propellant required, and this percentage is fixed by the rocket engine's theoretical efficiency. Payload, engines, propellant tanks, vehicle structures, and subsystems make up the remaining 10%. Fully reusable rocket designs must therefore carry nine times their weight in propellant and withstand the rigors of launch, entry, and recovery for a specified number of launches.

Figure 1 shows the effect of equivalent, effective specific impulse ( $I^*$ ) on the allowable dry weight fraction (including payload) for single-stage-to-orbit (SSTO).  $I^*$  is an integrated measure of system performance that accounts for propulsive efficiency, as well as all external forces encountered by the vehicle from lift-off to orbit. This makes it a relevant discriminator for systems where aerodynamic drag has a pronounced effect.  $I^*$  can be increased over that of a rocket by taking advantage of the higher specific impulse of air-breathing propulsion cycles over a portion of the ascent trajectory. For  $I^*$  equal to 650 seconds, the maximum allowable dry weight fraction increases to 30%, which seems to make the design of a reusable vehicle more tractable. For a given  $I^*$ , the amount of "excess dry weight" will depend on the weight burden of the air-breathing system. Excess dry weight could be used to build in higher reliability, increase the payload, or reduce the GLOW.

Factors that tend to increase the dry weight fraction of air-breathing launch vehicles include a lower thrust-to-weight ratio than rockets and a requirement that the vehicle accelerate within the atmosphere. This may result in pressure and thermal loads on the entire vehicle that exceed those of reentry. The bulk density of the propellant is

also reduced if hydrogen fuel is used in air-breathing modes. This can compound the aerodynamic drag and structural weight issues. The severity of these factors, as well as the dry weight fraction benefit, depends on the air-breathing velocity range, the trajectory flown, and the degree of integration between the vehicle and propulsion system. The design objective is thus to optimize  $I^*$  for a maximum dry weight margin, not to maximize  $I^*$ .

To quantify the system benefits of air-breathing propulsion is a considerable multidisciplinary undertaking. A candidate concept must be matured through preliminary design in order to accurately assess the dry weight with specified safety factors. This requires detailed propulsion, thermal, aerodynamic, and trajectory modeling. Results of the National Aero-Space Plane (NASP) program<sup>1-3</sup> provide insight into high  $I^*$  systems. NASP was a lifting-body configuration designed for airlineline operation from conventional runways. As a result, both the vehicle aerodynamics and landing gear were designed to support the GLOW. It employed a high-efficiency, but complex and heavy, low-speed propulsion unit. The fuselage shape was biased toward efficient high-Mach number scramjet operation, as opposed to structural efficiency. Positive dry weight margin could not be guaranteed for this class of vehicle at the conclusion of the NASP program.

NASA's X-33 program<sup>4</sup> provides recent insight into SSTO rocket issues. X-33 was to develop technologies leading to the "Venture Star"<sup>5</sup> reusable SSTO rocket. Advanced linear-aerospike engines provided an incremental advantage in  $I^*$  over a conventional rocket, but the dry weight margin was still elusive as the program was terminated last year.

It seems that the "jump" to air-breathing is required to enable reusable SSTO. However, it must be judiciously applied and highly integrated, both structurally and aerodynamically, with the vehicle. This forms the basis for the GTX reference vehicle configuration and performance goals. Initial conceptual studies<sup>6</sup> indicated that an  $I^*$  of roughly 500 seconds was feasible for an air-breathing, vertical lift-off, axisymmetric vehicle accelerating to moderate Mach numbers in the atmosphere and using rocket propulsion for low speed and vacuum operation. The "middle-class" GTX would fill the gap in knowledge between Venture Star<sup>5</sup> and NASP. It would take advantage of air-breathing efficiency, yet be more rocketlike in configuration, so as to increase the potential to meet the 20% dry weight fraction goal.

The objective of the GTX program is to determine whether or not air-breathing propulsion can enable reusable SSTO. Validation of the goal point on figure 1 would provide the basis for an operational vehicle and initiate evolution to even higher performance as new technology becomes available and as  $I^*$  optimization is better understood.

To validate the structural mass fraction and  $I^*$  goals, the program philosophy was to quickly develop a practical "reference vehicle" configuration and resist modifications to it, unless it became apparent that the performance goals could not be met. A reference vehicle is required for the integration and optimization necessary to enable SSTO. It provides a common basis for all discipline efforts and ensures the relevance of each. Development and flight testing of "rocket-based combined-cycle" (RBCC) engines in the absence of a system framework may lead to flawed conclusions regarding the feasibility of air-breathing launch vehicles. Detailed engineering and experimentation is favored over configuration trade studies, whose validity is tenuous anyway without the more detailed data. This paper presents an overview of the GTX reference vehicle and the approach to its performance validation. Levels of validation from component performance to flight demonstration are discussed.

## SYMBOLS

A	Cross-sectional area
$C^*$	Characteristic exhaust velocity
$C_f$	Combustor skin friction coefficient
$C_{fg}$	Thrust coefficient. Ratio of actual to reference thrust.
$C_D$	Vehicle drag coefficient
D	Vehicle drag
$I^*$	Equivalent, effective specific impulse
$I_{eff}$	Effective specific impulse. Ratio of the sum of all forces acting on a vehicle to the total propellant rate of flow.
$I_{net}$	Net propulsive specific impulse. Ratio of net thrust to total propellant flow.
M	Mach number
O/F	Ratio of oxidizer-to-fuel mass
$P_t$	Total pressure
$T_{net}$	Net thrust as defined by a control volume extending from the spike tip to the vehicle trailing edge.
$T_{max}$	Maximum temperature
W	Vehicle weight
V	Velocity
$\gamma$	Flight path angle
$\Delta$	Change in parameter
$\eta_c$	Combustion efficiency

### Subscripts

i	Trajectory segment
0	Free stream
1	Station 1—inlet spike tips
2	Station 2—inlet throat
4	Flow state following compression process
5	Flow state following combustion process
9	Station 9—nozzle exit projected area
C	Cowl lip projected area

## GTX REFERENCE VEHICLE

The GTX reference vehicle configuration, pictured in figure 2, is based on taking optimum advantage of air-breathing propulsion; that is, to maximize system performance by considering propulsion, weight, and simplicity in conceptual design. Table 1 gives basic specifications and operating limits. Vertical lift-off and horizontal landing minimizes the weight and complexity associated with horizontal takeoff and eliminates runway length, load, and lift-off speed issues. Hydrogen fuel was chosen based on its energy per unit mass and cooling capacity. Its low density, however, negatively impacts aerodynamic drag, structural weight, and packaging. The axisymmetric body is intended to mitigate these factors by providing good potential for lightweight, durable structure, volumetrically efficient propellant tanks, low transonic drag, and some measure of inlet precompression at hypersonic speeds. Three semicircular pods house the combined-cycle propulsion systems. These are oriented at 120° intervals and are offset from the vehicle surface to allow for diversion of the forebody boundary layer. This arrangement also results in thrust symmetry, which minimizes trim drag. The pods also provide an efficient attachment point for the wings and tail, away from the propulsive stream. In this arrangement, they contribute to the total vehicle planform area, and their stiff, circular ring frames carry wing loads through to the primary fuselage structure. See reference 6 for additional details on configuration rationale.

The reference vehicle is sized at a minimum useful scale to minimize the cost and development risk of the first air-breathing SSTO launch vehicle. Although this results in a meager payload fraction, it makes relevant flight demonstration vehicles more affordable. Scaling to larger payloads is feasible without significant change to the basic configuration.<sup>7</sup>

### PROPULSION SYSTEM AND OPERATING MODES

A cutaway view of the combined-cycle propulsion system is shown in figure 3. A translating centerbody provides the required variable geometry, with minimal sealing and actuation issues. The single thruster design favors light weight and simplicity over mixing between the rocket and air streams, which would require a longer flow path or multiple thruster elements. A number of hydrogen fuel injection stations provide for optimum ram and scramjet operation. The thruster nozzle is scarfed to provide pressure compensation during low altitude operation. The vehicle's sculpted aft region provides a common altitude-compensating expansion surface for the thruster and air-breathing exhaust streams. Flow path stations are defined as follows: station 0 represents the undisturbed free stream; station 1 defines the propulsion control-volume inflow and is located at the inlet spike tips; station 2 denotes the flow path minimum area; station 3 is the minimum nacelle radius and also the axial position of the thruster nozzle exit; station 6 is the trailing edge of the nacelle and also the maximum cross-sectional area in the flow path; and station 9 is the trailing edge of the vehicle, which represents the projected area available for nozzle expansion.

The propulsion system operates in the four modes pictured in figure 4. At lift-off in mode I, the required thrust is provided by the rocket at maximum chamber pressure. The inlet admits airflow to ventilate the flow path and prevent overexpansion of the thruster. As the vehicle accelerates and the ramjet stream gains thrust potential, it is fueled in the inlet diffuser, then ignited and piloted by the rocket exhaust. Thruster chamber pressure is controlled within limits to optimize the proportion of rocket to ramjet thrust. The transition to mode II occurs at about Mach 2.5 when ramjet thrust alone can sustain optimum acceleration. The interaction between the rocket and air streams, flashback to the fuel injectors, and overall performance in mode I are key issues to be addressed.

In mode II the propulsion system operates as a thermally choked ramjet. The inlet is started, and the thruster is off. Optimum performance dictates that the thermal throat moves upstream in the diverging flow path as flight Mach number increases. Inlet operability and control of the thermal throat location are the key issues in this mode.

Transition to mode III (scramjet mode) occurs at about Mach 5.5, due to the waning relative energy input due to combustion and increasing duct pressures. Fuel injection and combustion now occur just aft of the inlet throat. Thrust per unit airflow decreases with flight Mach number in this regime. At about Mach 11, a transition to mode IV is initi-

ated. Adequate combustion efficiency and nozzle performance must be demonstrated during preliminary validation of mode III.

In mode IV, the inlet centerbody is translated fully aft to close off the air-breathing flow path completely, forming an annular cavity upstream of the thruster. The entire flow path area ratio including the vehicle base is used for mode IV vacuum operation. The unconfined expansion at station 3 is managed by pressurizing the annular cavity with a small amount of inflow bleed. The thruster must be throttled in mode IV due to acceleration constraints. Combustion and expansion efficiency and the required amount of inflow bleed are key issues.

From lift-off to orbit, the propulsion system must be power balanced. This is complicated by the intermittent, variable chamber pressure operation of the thruster and the unsteady nature of the air-breathing flow path's heat load. Variations on expander and gas generator cycles that satisfy these requirements are described in reference 10. The VITMAC<sup>9</sup> computer program has also been developed to quickly screen candidate propellant system concepts and perform trade studies.

## MATERIALS AND STRUCTURAL ARCHITECTURE

Major elements of the vehicle structural architecture and materials are shown in figure 5. The nonintegral tank arrangement is designed to isolate the propellant tank stack and payload from the high-temperature aerodynamic environment during air-breathing ascent and reentry. This design accommodates the strain from all external loads as well as that due to cryoloading. The propellant tank stack is supported by a deep ring frame and articulated struts.<sup>9</sup> The propellant tank stack and payload bay are constructed with polymer-matrix composite (PMC) materials. The hydrogen tank is insulated with Airex<sup>®</sup> foam insulation. The aeroshell is constructed of carbon/silicon carbide (C/SiC) sandwich panels mounted to a carbon/carbon (C/C) substructure. Saffil<sup>®</sup> insulation backs the aeroshell to protect the PMC substructure. These material systems were chosen for their high-temperature strength and durability.

Figure 6 shows the materials and structural architecture of the propulsion systems. In general, surfaces with a view factor to space do not require active cooling.<sup>10</sup> Flow path internal surfaces are regeneratively cooled using the innovative heat exchanger architecture described in reference 10. Ceramic matrix composites (CMC's) are used for both applications. CMC's reduce the structural weight and increase the component operating temperature beyond that possible with metals.

## REFERENCE VEHICLE PERFORMANCE

The trajectory optimization method of reference 11 was used to maximize I\* based on input propulsion and aerodynamic characteristics. Mode 1 performance was estimated using the method of reference 12. Modes II and III were evaluated using the Ramjet Performance Analysis program.<sup>13</sup> Mode IV performance was estimated based on the results of reference 14. The Aerodynamic Preliminary Analysis System (APAS)<sup>15</sup> was used to calculate the lift and drag coefficient as a function of flight Mach number and angle-of-attack. The resulting I\* is 503 seconds at a vehicle oxidizer-to-fuel ratio (O/F) equal to 2.4.

Figure 7 presents specific impulse as a function of flight Mach number for the resulting optimal trajectory. The net specific impulse ( $I_{net}$ ) is based on a control volume extending from the inlet spike tips to the vehicle trailing edge. The effective specific impulse ( $I_{eff}$ ) is based on all forces acting on the vehicle. It is related to  $I_{net}$  in the following manner:

$$I_{eff} = I_{net} \left( 1 - \frac{D}{T_{net}} - \frac{W \sin(\gamma)}{T_{net}} \right) \quad (1)$$

$I_{net}$  and  $I_{eff}$  are strong functions of velocity. The system-level performance parameter ( $I^*$ ) is defined by the rocket equation in terms of the vehicle mass ratio and total  $\Delta V$ . However, it can be written in terms of  $I_{eff}$ :

$$I^* = \frac{\Delta V}{\int_{\Delta V} \frac{dV}{I_{eff}}} \quad (2)$$

A validation of  $I_{eff}$  over the velocity range can thus represent a level of  $I^*$  validation. In turn, a validation of  $T_{net}$ ,  $I_{net}$ , and vehicle drag at a given flight condition could be considered a validation of  $I_{eff}$  at that point.

The Mach number range in figure 7 has been partitioned into six segments, and the equivalent, effective specific impulse for each segment ( $I_i^*$ ) is shown. These constants represent the variable  $I_{eff}$  for a given range. Using these six constants, the integral in equation (2) becomes a summation, and the sensitivity of  $I^*$  to a change in  $I_{eff}$  over a particular segment can be evaluated:

$$\frac{\Delta I^*}{\Delta I_{eff,j}} = \left( \frac{I^*}{I_{eff,j}} \right)^2 \left( \frac{\Delta V_i}{\Delta V} \right) \quad (3)$$

Sensitivities based on equation (3) appear in figure 8.  $I^*$  is most sensitive to mode IV performance, due to the relatively low specific impulse and high  $\Delta V$ . Note that these sensitivities and those in subsequent figures are based on a 1% variation in the independent variable.

## REFERENCE VEHICLE SIZING AND STRUCTURAL WEIGHT

Maturation of the reference vehicle is done in an iterative fashion, due to the strong interdependence between aeropulsion performance, structural architecture, and the trajectory flown. The vehicle and propulsion system structures are designed and optimized based on the loads from the latest trajectory. Reference 10 presents the structural analysis used to insure adequate margins of safety. The vehicle is then scaled to the point where the propellant fraction matches that required. A preliminary sizing model<sup>16</sup> was developed to facilitate this process. It uses scaling laws specific to the reference vehicle structural architecture to determine the GLOW, based on the required propellant fraction, O/F, margins, and payload. The sizing model is updated regularly to reflect any changes to the structural architecture and the results of analytical and experimental validation efforts. Figure 9 shows the effects of scale on gross lift-off weight based on the latest modeling. Based on an  $I^*$  of 503 seconds and an O/F of 2.4 the vehicle gross lift-off weight is 690,000 lb. Note that to reduce GLOW,  $I^*$  must be increased without reducing O/F. For example, extending the air-breathing Mach number range increases  $I^*$  but reduces O/F and may actually increase the GLOW. Increasing the efficiency of an air-breathing mode, however, will increase  $I^*$  and O/F and have a much more significant impact on GLOW.

A structural weight summary for this case appears in table 2. The air-breathing propulsion systems account for almost one-fourth of the dry weight. Sensitivity of GLOW to dry weight uncertainty is shown in figure 10. A 15% uncertainty will double the gross weight. Therefore it is critical to avoid excessive safety factors and dry weight margin by striving to increase the accuracy of structural modeling.

## PERFORMANCE VALIDATION APPROACH

A successful demonstration of Technology Readiness Level (TRL) 7—"System Prototype Demonstration in a Space Environment"<sup>17</sup> will prove the feasibility of a reusable SSTO and would bring the GTX program to a close. This level of system validation is achieved in steps, each step reducing the risk of the next. The GTX TRL 7 demonstration would consist of flight from lift-off through the mode III-IV transition with effective specific impulse and unit weights at goal levels. Since only one-half of the total  $\Delta V$  is required, this can be accomplished with a subscale vehicle, using materials and architectures similar to those of the reference vehicle. The scale could be further reduced by demonstrating this  $\Delta V$  in a number of segments. As scale and  $\Delta V$  are reduced however, structural architecture, wing loading, and dynamics will depart from those of the reference vehicle. Procedures that relate flight demonstration results to the reference vehicle scale are thus a critical part of the validation process.

Validation of reference vehicle performance to TRL 5-6 consists of propulsion system ground demonstration and limited flight demonstration. The flight demonstration validates airframe-integrated propulsion performance at scale and Mach numbers not practical on the ground and serves as the initial phase of the TRL 7 flight program.<sup>18</sup> The propulsion system ground demonstration (see "rig 5" below) validates uninstalled propulsion performance, structural weight and integrity, and power-balanced operation. As in the TRL 7 validation, results of these experiments must be related to the reference vehicle. Computational fluid dynamics (CFD) analysis will also be required to quantify scale and integration effects.

Validation to TRL 3-4 is accomplished by defining the component efficiencies necessary to meet the reference vehicle performance goals and by demonstrating these efficiencies over the relevant  $\Delta V$  range. Obviously, more reliance on various analysis disciplines (cycle, aerodynamic, structural, trajectory, etc.) is inherent at this level of validation, and it is considered preliminary. A series of test rigs has been identified for component development and validation. CFD is used extensively for component design as well as interpretation and extrapolation of experimental results.

## COMPONENT DEVELOPMENT AND VALIDATION

This section reviews the test rigs and associated CFD analysis used for component development and validation. Figure 11 presents the matrix of rigs by component and speed range. As explained below, rig 5 is a propulsion system test rig, and would cover as much of the matrix as practicable in ground facilities. This suite of test rigs provides most of the information necessary for preliminary validation. Vehicle-integrated mode III information is limited by the scale and Mach number available in ground facilities and is a candidate objective for initial flight demonstrations. The role of CFD is threefold: 2-D or simplified models such as the method of characteristics are used for aerodynamic design; more sophisticated 3-D and or reacting flow models are used for pretest predictions and to aid in interpreting experimental results, especially in cases where instrumentation may be sparse; and finally, CFD is instrumental in relating test results to the reference vehicle. It is often impractical to match the test conditions, test medium, and scale in component rigs.

### RIG 1: DIRECT-CONNECT MIXER-COMBUSTOR

The primary objective of this rig is to develop the low-speed operating modes of the flow path and to evaluate the performance of the resulting scheme. The rig is designed to study the effects of combustor length, thruster geometry, and pressure ratio on the mixing between the rocket and air streams as well as the resulting effects on overall performance. A variety of flush-wall and in-stream gaseous hydrogen fueling stations are included to develop and evaluate both the airstream fueling scheme and the transition from modes 1 to 2 as the rocket thruster is shut off. Rig 1 also provides a relevant environment for coupon and subcomponent tests of proposed materials and cooling systems.

Rig 1 is a connected-pipe model of the flow path, from the inlet throat to the combustor exit, including a hydrogen-oxygen rocket thruster. It is installed in the Engine Components Research Laboratory<sup>19</sup> at NASA Glenn Research Center (GRC), which can supply unvitiated inflow air at conditions from sea-level static to Mach 3. Checkout of the propellant and safety systems has been completed. A total of 20 mode I tests consisting of 5-second rocket firings have been accomplished to date. See reference 20 for additional details. Two-dimensional CFD studies of mode I operation have been done in conjunction with rig 1 planning and are reported in references 21 and 22.

### RIG 2: INLET DEVELOPMENT AND VALIDATION

The objectives of rig 2 testing are to develop a mixed-compression inlet design that has the potential for light weight and minimum complexity, is operable over the required Mach number range, and satisfies vehicle integration and mode IV flow path closure constraints. Performance results are used to validate cycle analysis modeling based on 2-D CFD.<sup>23</sup> Data are also obtained to validate 3-D CFD modeling used to extend results beyond the Mach and Reynolds number limitations of ground test facilities.

Rig 2 is a 2.65-in. cowl lip radius aerodynamic model of the inlet from the spike tip to station 3. The model has a remotely controlled spike and mass flow plug. It also has a number of interchangeable features including end-wall boundary-layer bleed and diverter geometry. Rig 2 is installed in the 1- by 1-Foot Supersonic Wind Tunnel<sup>24</sup> at NASA GRC and is designed for operation from Mach 2.5 to 6.

Two phases of rig 2 testing have been completed, along with initial 3-D calculations of the latest configuration. In the first phase,<sup>25</sup> maximum contraction ratios and inlet performance were below those required to achieve the system performance goal. The inlet contours were subsequently redesigned.<sup>23</sup> The most prominent changes were a reduction in the spike angle from 12° to 10° and a reduction in the throat angle from 15° to 12°. Performance near the goal levels was demonstrated with this configuration.<sup>26</sup> Reference 26 also shows, using 3-D Navier-Stokes calculations, that slight shortfalls in recovery and contraction ratio are due to Reynolds number effects. These results give sufficient confidence to proceed with vehicle-integrated inlet testing (see rig 3 below). Further isolated inlet tests of the rig 2 variety are not planned.

### RIG 3: FOREBODY-INLET INTEGRATION

Rig 3 is intended to investigate forebody-inlet and pod-to-pod interactions and also the effects of angle-of-attack on inlet operability and performance. It is a 6.620-in. cowl lip radius model of the GTX reference vehicle configuration, designed in a modular fashion to allow testing of various boundary-layer diverter configurations.

A first phase of testing has been completed in the GRC 10- by 10-Foot Supersonic Wind Tunnel<sup>27</sup> from Mach 2 to 3.5.<sup>28</sup> These tests incorporated three fixed inlet spikes extending aft only to the cowl lip plane to insure starting. The effects of vehicle angle-of-attack on captured air flow and cowl lip plane distortion were documented. Pitot and static pressure measurements and oil-flow visualization were also obtained for comparison to 3-D CFD modeling of the forebody.<sup>29</sup> There was no evidence of leeward-side flow separation, nor any sudden disruption of inlet flow over

the range of angle-of-attack and Mach number tested. The pylon-type boundary-layer diverters effectively isolated the inlets from the forebody boundary layer and its interaction with the conical shocks. Tests with the inlet mounted directly on the forebody surface (no diverter) showed a marked reduction in mass capture and an increase in distortion. These results give sufficient confidence to proceed with the second phase of tests where an actuated mixed-compression inlet similar to the latest rig 2 design will replace two of the three pods in succession to map inlet performance and operability limits as a function of vehicle angle-of-attack. Detailed design of the hardware for this phase of testing has been completed.

#### RIG 4: FLOW PATH DEVELOPMENT AND INTEGRATION

Rig 4 serves to develop and optimize the mode II and III fuel injection scheme in the presence of realistic inlet flow profiles. Combustor-inlet interactions are also properly characterized using the “free-jet” test approach. Uninstalled performance and operability of the evolving configuration is documented for use in anchoring 3-D CFD models<sup>22</sup> and cycle analysis.

Rig 4 is a 5.130-in. cowl lip radius hydrogen-fueled model of the flow path from the inlet spike leading edge to station 6. It is constructed largely of copper with water-cooled leading edges. The inlet centerbody is remotely controlled to allow starting and to vary the contraction ratio. Tests were conducted in Leg 4 of the Propulsion Test Complex at GASL.<sup>30</sup>

Similar to the initial rig 2 results, the anticipated maximum inlet contraction ratios were not achieved during the first phase of rig 4 testing. Consequently, as reported in reference 31, combustion efficiency and thrust performance were adversely affected. The current phase of testing incorporates the 10°-spike/12°-throat inlet design and additional fuel injection stations. In recent tests, this configuration operated successfully at Mach 7 at the design contraction ratio of 12.

#### RIG 5: FLIGHTLIKE INTEGRATED PROPULSION SYSTEM

Rig 5 serves to integrate flow path components, structures, materials, propellant subsystems, and controls into a propulsion system. It proceeds from successful component demonstration and will be conducted in phases of increasing complexity. Uninstalled net thrust, specific impulse, structural weight and integrity, and power-balanced operation will be validated over the maximum Mach number range practical for a ground test. The final phase of rig 5 work will run concurrently with flight demonstration, qualifying flight engines to a yet-to-be-determined extent. The scale chosen for the rig 5 demonstrators will be that of the initial flight demonstration vehicle, as long as this does not impact the range of ground test conditions. For example, reference 18 reports a 26%-scale demo vehicle with a cowl lip radius of 15.521 in. Hypersonic ground test facilities do exist that would accommodate this scale engine,<sup>32, 33</sup> but it may be more cost effective to do initial demonstrations at a smaller scale.

#### RIG 6: ROCKET ELEMENT DEVELOPMENT

The GTX propulsion system concept employs a single thruster in each flow path. For optimal system performance this thruster must have high combustion efficiency over a wide throttle range and a pressure-compensating nozzle design. It must be well integrated both structurally and aerodynamically with the flow path. Rig 6 experiments will ultimately be used to validate the construction and performance of flight-weight thrusters for their use in rig 5 testing and flight demonstration. Initially, rig 6 has been used to develop the thruster element for rig 1.

The rig 1 thruster is water cooled and has a 1-in. diameter throat. It is designed for gaseous hydrogen and gaseous oxygen propellants at a maximum chamber pressure of 1500 psia and O/F of 4 to 6. It was tested at the GRC Research Combustion Lab Cell 32<sup>34</sup> from 300 to 750 psia at O/F of 4 and 6. Testing was limited to chamber pressures below 750 psia due to cooling concerns. Characteristic exhaust velocities ( $C^*$ ) 91 to 96% of ideal were observed. Subsequent analysis indicated that the design had adequate cooling, and it was deemed acceptable for installation into rig 1. In the absence of any thruster issues during rig 1 tests, subsequent rig 6 testing awaits further maturation of the reference vehicle and flight demonstration engine designs.

#### RIG 7: ROCKET-IN-A-DUCT CODE VALIDATION

In the GTX propulsion concept, the thruster is integrated with the flow path such that maximum advantage is taken of the high-area-ratio air-breathing duct during mode IV operation. The thruster stream must, however, negotiate a region of “free expansion” across the duct at station 3. It is important to understand this process, since system performance is highly sensitive to mode IV efficiency. The objective of rig 7 is to investigate the effects of area ratios, length, and secondary flow on the expansion efficiency of a generic, axisymmetric rocket-in-a duct.

Tests were conducted in the GRC Research Combustion Lab Cell 11<sup>35</sup> with a small (25-lb. class), hydrogen-oxygen thruster. Results of these tests<sup>36</sup> corroborated axisymmetric CFD analysis, which was used to develop an expansion efficiency correlation used for preliminary flow path design and cycle analysis.<sup>14</sup> It was found that a small amount of bleed flow (roughly 1% of the total propellant flow) effectively manages the free expansion by pressurizing the cavity upstream of the thruster exit.

#### RIG 8: NOZZLE PERFORMANCE

In keeping with the desire for light weight and simplicity, the GTX nozzle has a fixed geometry and is highly integrated with the vehicle. This, coupled with the various modes in which the propulsion system operates, results in somewhat lower performance and greater uncertainty than for traditional rocket or jet engine nozzles. The objectives of rig 8 are to develop the nozzle design, validate expansion efficiency, and provide data for comparison to 3-D CFD models over the entire range of operating conditions. For modes I and IV, the thruster flow must be simulated. Modes I to III require modeling of the ramjet stream, with either a thermal throat or supersonic inflow condition at various stations and area ratios within the flow path.

A subscale model of the flow path from the inlet throat to the vehicle trailing edge has been designed to efficiently obtain performance data in all modes.<sup>37</sup> The flow contours are based on the current GTX reference vehicle flow path, which has a continuous 12° conical expansion from the thruster throat to the vehicle trailing edge and a 7.86° conical nacelle between stations 3 and 6. This design is evolved from that of reference 38, based on the 3-D CFD analysis reported therein. The Aero Systems Engineering (ASE) Channel 8 static test stand<sup>39</sup> is being considered for testing in modes I to III. The rig would be moved to ASE's Channel 9<sup>40</sup> facility for mode IV tests. Detailed design as well as structural and thermal analyses have been completed for this rig. 3-D CFD calculations are being conducted for the lift-off (mode I), Mach 10 (mode III), and mode IV cases. The status of these calculations is reported in reference 37.

#### RIG 9: HIGH MACH PERFORMANCE VALIDATION

High-Mach-number air-breathing performance is difficult to validate due to the scale and enthalpy limits of current ground test facilities. Pulse facilities offer an economical way to obtain data at high Mach number. The objectives of rig 9 testing are to develop and optimize the fuel injection strategy in the high mode III range, provide data for comparison to CFD calculations,<sup>22</sup> and provide flow path performance information. An additional objective is to collect data at Mach 7 for comparison to steady-state rig 4 results.

Tests were conducted in the Hypulse<sup>30</sup> facility at GASL. Hypulse is a shock tunnel capable of simulating Mach 7-10 in reflected shock mode. The 5.130-in. cowl lip radius model is constructed mainly of aluminum, with stainless steel leading edges and fuel manifolds. The flow path geometry is similar to the latest rig 2 and 4 configurations with a 10° spike and 12° throat. The inlet spike is fixed at the design contraction ratio of 12. Tests have been conducted at Mach 7 and 10 conditions.<sup>41</sup>

#### AXISYMMETRIC RBCC TEST RIG

An augmentation to an internal research and development program at the Johns Hopkins University Applied Physics Laboratory has led to an interesting series of experiments on a fully round version of the GTX flow path. These tests are intended to allow relatively inexpensive parametric testing and to provide fully axisymmetric data for comparison to other rigs and CFD.

The 2.5-in. cowl lip radius heat-sink model is being tested in the Free-jet Engine Facility at the Avery Advanced Technology Development Center.<sup>42</sup> The inlet contours mirror those of the other flow path rigs with a 10° spike and 12° throat. Downstream of station 3 and in the thruster nozzle, the flow path area ratios have been matched approximately. The thruster is fueled by a mixture of hydrogen and enriched air. Sea-level static (Mode I) and near-vacuum (Mode IV) tests are planned. Inlet aerodynamic tests have been completed using the facility's Mach 4 free-jet nozzle. See reference 43 for additional details.

### BASELINE COMPONENT PERFORMANCE AND SENSITIVITIES

Key air-breathing component and mode IV efficiency assumptions that underlie the reference vehicle I\* goal are presented in this section. These are the "design" levels to be validated with test rigs and CFD. The sensitivity of I\* to a 1% change in a given parameter over each trajectory segment is also shown. This information is used to assess the status of a given component's development and to prioritize development and validation efforts.

## AIR CAPTURE

Figure 12a shows the assumed air flow characteristics for the reference vehicle. The mode I air flow is limited either by a thermal throat or by choking in the inlet. The mode II and III capture characteristics are based on 2-D (axisymmetric) CFD calculations of the forebody and inlet described in reference 23. The Mach 6 shock-on-lip design point for the inlet is evident in the  $A_1/A_C$  trace. The  $A_0/A_C$  trace shows the increased mass capture due to vehicle forebody compression. Recent test data from rigs 2 and 3<sup>26,28</sup> fall slightly below the baseline. This is attributed to Reynolds number and 3-D effects. Validation of the  $A_0/A_C$  levels would require high-speed rig 3 or flight testing. Figure 12b shows the sensitivity of  $I^*$  to a 1% change in air capture. For example, a 10% shortfall in mass capture over the high mode II range would result in a 5.5-second reduction in  $I^*$  and a concomitant reduction in dry weight allowance.

## INLET RECOVERY

Inlet recovery levels based on the reference 23 results, and the sensitivity of  $I^*$  to recovery appear in figure 13. The discontinuities at Mach 2.5 and 5.5 are due to inlet starting and mode II-III transition respectively. Recovery based on the free stream total pressure includes losses due to the vehicle forebody and is used in cycle analysis to determine the state following the compression process. Recovery based on station 1 is plotted for comparison to isolated inlet tests and higher fidelity CFD calculations. The rig 2 data shown falls below the baseline due to Reynolds number and 3-D effects described in reference 26. The sensitivity of  $I^*$  to total pressure recovery is greatest during mode I because the inlet is unstarted. As a result, recovery affects the air flow, spillage drag, and the degree of nozzle over-expansion. In the low range of mode III, the sensitivity is negligible because changes in recovery are compensated by Rayleigh losses as the combustor inlet Mach number varies.

## INLET CONTRACTION RATIO

Geometric and aerodynamic contraction ratios are plotted in figure 14. The aerodynamic contraction ratio is reduced by spillage for Mach number less than 6 and increased by forebody compression as the Mach number increases. The maximum contraction ratios obtained during rig 2 tests<sup>26</sup> with roughly 2% end-wall bleed fall slightly below the baseline at the lower Mach numbers, again likely due to scale. If bleed is required at reference vehicle scale, the effect on  $I^*$  will be minimal, based on the sensitivity of  $I^*$  to a small reduction in airflow during mode II. The sensitivity of  $I^*$  to contraction ratio is low because the design contraction ratio of 12 is near optimum for the GTX reference vehicle configuration at high Mach. The sensitivity for the low mode III range is even lower because of the relatively high specific impulse over this range. The contraction ratio shown for mode II is that required for ramjet operation based on the 2-D CFD study.<sup>23</sup>  $I^*$  sensitivity was not calculated for mode II due to a lack of information at other contraction ratios. However, as long as the inlet remains started, sensitivity would be low, since sensitivity to recovery and air capture is minimal.

## COMBUSTION EFFICIENCY

For a given air flow, the combustion process in the various modes is characterized by a combustion efficiency, a friction coefficient to account for momentum loss, and a cross-sectional area ratio over which the process occurs. A stoichiometric fuel-air ratio is currently assumed in modes II and III, although this is not necessarily optimal. The fuel-air ratio varies in mode I as a function of flight Mach number. A combustion efficiency of 92.5% was assumed for all air-breathing modes. Recent rig 9 tests<sup>41</sup> achieved stoichiometric combustion efficiencies of 94 and 89% at Mach 7 and 10 respectively, indicating that the baseline level is reasonable, especially for the reference vehicle scale. Testing rigs 1 and 4 will serve to develop and validate the fuel injection scheme at the lower Mach numbers. Figure 15 shows the sensitivity of  $I^*$  to changes in combustion efficiency for the given trajectory segments. The sensitivity in the high range of mode III is more than twice that of the other segments because of the relatively low specific impulse in this range.

## COMBUSTOR FRICTION COEFFICIENT

A friction coefficient of 0.0025 was assumed for all modes. This is a constant, equivalent value used to represent the momentum loss due to wall friction. Figure 16 presents the sensitivity of  $I^*$  to friction coefficient. The sensitivity is very low, but uncertainty in this parameter is high due to the lack of CFD or experimental results to date. Information in the high mode III range would be of the greatest value.

## COMBUSTOR EXIT AREA

Figure 17a shows the cross-sectional area at which combustion is assumed to be complete. In general, the trend is for this area to decrease with increasing flight Mach number. In modes I and II,  $A_5$  represents the thermal throat area and affects the air flow rate. In an expanding flow path,  $A_5$  depends on the axial station at which combustion is complete and is controlled by affecting fuel distribution, mixing, and flame holding. As a result,  $A_5$  is both difficult to design for and to measure in experiments. The effect of  $A_5$  perturbations on  $I^*$  is shown in figure 17b. In mode I, a reduction in  $A_5$  results in reduced air flow, increased inlet drag, and more severe nozzle over-expansion. In modes II and III, the sensitivity is of lesser magnitude and opposite sense, as a reduction in  $A_5$  increases performance due to reduced Rayleigh losses. Rigs 1, 4, and 9 are intended to develop the operational strategies for controlling  $A_5$ . Validation of  $A_5$ , like the friction coefficient, will be inferred from validation of uninstalled net thrust.

## NOZZLE GROSS THRUST COEFFICIENT

Gross thrust coefficient ( $C_{Tg}$ ) is used as the measure of expansion efficiency and is defined as the ratio of measured gross thrust to a reference value. The reference value for mode I is the thrust function evaluated at station 6. For modes II and III it is based on isentropic, equilibrium expansion to free stream pressure. The  $C_{Tg}$  assumed for mode I is 0.90. For modes II and III, 0.95 is used. As seen in figure 18,  $I^*$  is highly sensitive to the expansion efficiency defined in this manner. A 1% change in  $C_{Tg}$  over the high mode III range would result in a 6-second change in  $I^*$ . Rig 8 and its associated computational effort will serve to develop the highly integrated multimode configuration and validate its efficiency.

## MODE IV PERFORMANCE

The mode IV performance shown in figure 7 is based on a thruster  $C^*$  efficiency of 94 to 98% depending on chamber pressure and an expansion efficiency of 94%. The expansion efficiency is based on isentropic, equilibrium expansion from the thruster throat to  $A_9$ . A 1% shortfall in either parameter results in an equivalent shortfall in mode IV vacuum specific impulse. Therefore, the sensitivity of  $I^*$  to either parameter equals that shown in figure 8, 3.344 seconds. Rig 6 is intended for development and validation of the high-efficiency, variable chamber pressure thruster. Expansion efficiency of the unique, integrated configuration with its secondary flow and aft-body expansion will be validated using rig 8. Rig 7 is available to further research the "rocket-in-a-duct" physics, should that become necessary to meet the performance goals.

## VEHICLE DRAG

Another important factor in the determination of system performance is the aerodynamic characteristics of the vehicle. The drag coefficient over the optimal trajectory is plotted in figure 19.  $I^*$  is most sensitive to vehicle drag in the high mode III range where the difference between thrust and drag is minimum. Current plans call for validation of these APAS results using 3-D CFD.

## VALIDATION OF STRUCTURAL ARCHITECTURE AND WEIGHT

Validation of the structural architecture and weight is a multidisciplinary activity. First, the dynamic, pressure and thermal loads are evaluated for the ascent and reentry trajectories<sup>9</sup>. Critical load cases are selected for further analysis to verify the integrity of and optimize the structure. Structural response to the critical loads is evaluated using NASTRAN<sup>44</sup> finite element analysis. These results are used to determine factors of safety for the primary structure and to develop weight models.

## MATERIAL PROPERTY VERIFICATION

Advanced materials are required to meet the dry weight goal at a practical GLOW. For example, the flow path incorporates C/SiC heat exchangers and a C/C substructure. These materials have thermal and mechanical properties well suited to the high-speed air-breathing propulsion application but are at a relatively low TRL. The inclusion of low-TRL materials in the design drive the need for basic material property verification. To this end, Pratt & Whitney has begun a bank of materials screening tests.<sup>45</sup> In addition, Pratt & Whitney has performed a subscale, proof-of-concept test on the innovative, lightweight heat exchangers proposed for flow path regenerative cooling.<sup>46</sup> The concept is aggressive and demands early verification. This architecture is currently being scaled up to a 2.5-in. by 10-in. panel to be tested at GRC in 2002. Future plans include testing of a larger component in a more relevant environment at the United Technologies Research Center SCRAMJET test facility. Other candidates for material property and processing verification include large-scale C/SiC sandwich panels and large-scale C/C structural framework.

## CONCLUDING REMARKS

Validation of an air-breathing launch vehicle must be done at the system level for all propulsion modes. This insures the relevancy of technology development and brings to light issues that may prevent a given approach from being successful. To this end, the GTX program has focused on the reference vehicle presented herein with little change in configuration since 1997. A substantial database of experimental and analytical results has been assembled for both aeropropulsion and structural characteristics of the reference vehicle and propulsion system. Validation of the concept to TRL 3-4 is in progress. Given the high percentage of dry weight attributed to the flow path, material property tests to validate the C/SiC heat exchanger construction are of high priority. Rig 8 testing is also of high priority due to the sensitivity of  $I^*$  to mode IV performance and nozzle efficiency. Flight demonstration is required for system validation to TRL 7. A phased approach is proposed, where the first phase serves to validate mode II and III installed performance at speeds and scale not possible in ground test facilities.

## REFERENCES

1. Chase, R.L.; and Tang, M.H.: A History of the NASP Program from the Formation of the Joint Program Office to the Termination of the HySTP Scramjet Performance Demonstration Program. AIAA Paper 95-6031, 1995.
2. Sypniewski, C.: The NASP Challenge: Technical Breakthrough. AIAA Paper 89-5017, 1989.
3. Korthals-Altes, S.W.: Will the Aerospace Plane Work? Technology Review, vol. 90, no. 1, 1987, pp. 42-51.
4. Cook, S.A.: The Reusable Launch Vehicle Technology Program and the X-33 Advanced Technology Demonstrator. NASA TM-111868, 1995.
5. Baumgartner, R.I.: VentureStar Single Stage To Orbit Reusable Launch Vehicle Program Overview. Proceedings of the Space Technology and Applications International Forum – Second Conference on Next Generation Launch Systems, Albuquerque, NM, January 1997.
6. Trefny, C.J.: An Air-Breathing Launch Vehicle Concept for Single-Stage-to-Orbit. AIAA Paper 99-2730, 1999.
7. Roche, J.M.; and Kosareo, D.N.: Structural Sizing of a 25,000-lb Payload, Air-Breathing Launch Vehicle for Single-Stage-to-Orbit. Proceedings of the JANNAF 25th Airbreathing Propulsion Subcommittee Meeting, Monterey, CA, 2000.
8. Warburton, R.; and Wenzel, R.: Structures, Materials, and Thermal Management Contract—FR-25292-2. 2002.
9. Traci, R.; Walker, J.F.; and VanGriethuysen, V.A.: Thermal Management Analysis Tool for RBCC Propulsion Systems. Proceedings of the JANNAF 25th Airbreathing Propulsion Subcommittee Meeting, Monterey, CA, 2000.
10. Hunter, J.E.; McCurdy, D.R.; and Dunn, P.W.: GTX Reference Vehicle Structural Verification Methods and Weight Summary. Proceedings of the JANNAF 26th Airbreathing Propulsion Subcommittee Meeting, Destin, FL, 2002.
11. Hargraves, C.R.; and Paris, S.W.: Direct Trajectory Optimization Using Nonlinear Programming and Collocation. Journal of Guidance, vol. 10, no. 4, 1987.
12. Yungster, Shaye; Trefny, C.J.: Analysis of a New Rocket-Based Combined-Cycle Engine Concept at Low Speed. AIAA Paper 99-2393, 1999.
13. Pandolfini, Peter P.; and Friedman, Murray A.: Instructions for Using Ramjet Performance Analysis (RJPA). IBM-PC Version 1.24. The Johns Hopkins University Applied Physics Laboratory JHU/APL AL-92-P175, 1992.
14. Smith, T.D.; Steffen, C.J.; Yungster, S.; and Keller, D.J.: Analysis of a Rocket Based Combined Cycle Engine During Rocket Only Operation. NASA/TM—1998-206639/REV1, 1998.
15. Cruz, C.I.; and Willhite, A.W.: Prediction of High-Speed Aerodynamic Characteristics Using the Aerodynamic Preliminary Analysis System (APAS). AIAA Paper 89-2173, 1989.
16. Roche, J.M.; and McCurdy, D.: Preliminary Sizing of Vertical Take-Off, RBCC-Powered Launch Vehicles. Proceedings of the JANNAF 25th Airbreathing Propulsion Subcommittee Meeting, Monterey, CA, 2000.
17. NASA Technology Plan—Appendix B: <http://technologyplan.nasa.gov/default.cfm?id=AppB>
18. Krivanek, T.M.; Roche, J.R.; Riehl, J.; and Kosareo, D.: Affordable Flight Demonstration of the GTX Air-Breathing SSTO Vehicle Concept. Proceedings of the JANNAF 26th Airbreathing Propulsion Subcommittee Meeting, Destin, FL, 2002.
19. Colantonio, R.O.; Pachthofer, P.M.; Parrott, E.L.; and Piendl, B.R.: Advanced Combustor Rig at NASA Lewis Research Center's Engine Components Research Laboratory. NASA TM-4546, 1994.
20. Walker, J.F.; Thomas, S.R.; Krivanek, T.M.; Kamhawi, H.; and Smith, T.D.: Status of the RBCC Direct-Connect Mixer-Combustor Experiment. Proceedings of the JANNAF 26th Airbreathing Propulsion Subcommittee Meeting, Destin, FL, 2002.
21. Steffen, C.J.; and Yungster, S.: Computational Analysis of the Combustion Processes in an Axisymmetric, RBCC Flowpath. Proceedings of the JANNAF 25th Airbreathing Propulsion Subcommittee Meeting, Monterey, CA, 2000.

22. Steffen, C. J.; and Edwards, J.R.: Three-Dimensional CFD Analysis of the GTX Combustor. Proceedings of the JANNAF 26th Airbreathing Propulsion Subcommittee Meeting, Destin, FL, 2002.
23. DeBonis, J.R.; Steffen, C.J.; Rice, T.; and Trefny, C.J.: Design Evolution and Performance Characterization of the GTX Air-Breathing Launch Vehicle Inlet. Proceedings of the JANNAF 26th Airbreathing Propulsion Subcommittee Meeting, Destin, FL, 2002.
24. Seablom, K.D.; Soeder, R.H.; Stark, D.E.; Leone, J.F.X.; and Henry, M.W.: NASA Glenn 1- by 1-Foot Supersonic Wind Tunnel User Manual. NASA/TM—1999-208478, 1999.
25. DeBonis, J.R.; and Trefny, C.J.; Supersonic Wind-Tunnel Tests of a Half-Axisymmetric, 12°-Spike Inlet to an RBCC Propulsion System. Proceedings of the JANNAF 25th Airbreathing Propulsion Subcommittee Meeting, Monterey, CA, 2000.
26. Frate, F.C.; and Slater, J.W.: Supersonic Wind-Tunnel Tests of an Axisymmetric-Sector, 10°-Spike Inlet to a Rocket-Based Combined-Cycle Propulsion System. Proceedings of the JANNAF 26th Airbreathing Propulsion Subcommittee Meeting, Destin, FL, 2002.
27. Soeder, R.H.: User Manual for NASA Lewis 10- by 10-Foot Supersonic Wind Tunnel. NASA TM—105626, 1995.
28. Kim, H.D.; and Frate, F.C.; Experimental Evaluation of the Effect of Angle-of-Attack on the External Aerodynamics and Mass Capture of a Symmetric, Three-Engine Air-Breathing Launch Vehicle Configuration at Supersonic Speeds. Proceedings of the JANNAF 25th Airbreathing Propulsion Subcommittee Meeting, Monterey, CA, 2000.
29. Frate, F.C.; and Kim, H.D.: Wind Code Application to External Forebody Flowfields With Comparison to Experimental Results. AIAA Paper 2001–0226, 2001.
30. Roffe, G.; Bakos, R.; and Erdos, J.: The Propulsion Test Complex at GASL. ISABE 97–7096, 1997.
31. Thomas, S.R.; Saunders, J.D.; and Walker, J.F.: Mach 3.5 to 7 Free-Jet Tests of the GTX RBCC Flowpath with a 12°-Spike Inlet. Proceedings of the JANNAF 25th Airbreathing Propulsion Subcommittee Meeting, Monterey, CA, 2000.
32. Thomas, S.R.; Woike, M.R.; and Pack, W.D.: Mach-6 Integrated Systems Tests of the NASA Lewis Research Center Hypersonic Tunnel Facility. NASA TM–107083, 1995.
33. Kelly, H.N.; Wieting, A.R.: Modification of NASA Langley 8-Foot High Temperature Tunnel to Provide a Unique National Research Facility for Hypersonic Air-Breathing Propulsion Systems. NASA TM–85783, 1984.
34. Zoeckler, J.G.; Green, J.M.; and Raitano, P.: A New Facility for Advanced Rocket Propulsion Research. NASA TM–106193 (AIAA Paper 93–1859), 1993.
35. Arrington, L.A.; and Schneider, S.J.: Low Thrust Rocket Test Facility. AIAA Paper 90–2503, 1990.
36. Schneider, S.J.; and Reed, B.D.: Rocket-in-a-Duct Performance Analysis. AIAA Paper 99–2101, 1999.
37. Smith, T.D.; Rice, T.; Yungster, S.; and Blaha, B.J.: Integrated Nozzle Design for the GTX RBCC Flowpath. Proceedings of the JANNAF 26th Airbreathing Propulsion Subcommittee Meeting, Destin, FL, 2002.
38. Smith, T.D.; Lam, D.; Canabal, F.; and Rice, T.: Development of an Integrated Nozzle for a Symmetric, RBCC Launch Vehicle Configuration. Proceedings of the JANNAF 25th Airbreathing Propulsion Subcommittee Meeting, Monterey, CA, 2000.
39. Flugstad, T.H.; Romine, B.M.; and Whittaker, R.W.: High Mach Exhaust System Concept Scale Model Test Results. AIAA Paper 90–1905, 1990.
40. Mikkelsen, K.L.; and Idzorek, J.J.: Experience in the Operation of a Hypersonic Nozzle Static Thrust Stand. AIAA Paper 92–3292, 1992.
41. Thomas, S.R.; and Capriotti, D.P.: Mach 7 to 10 Free-Jet Engine Tests of the NASA GTX RBCC Flowpath. Proceedings of the JANNAF 26th Airbreathing Propulsion Subcommittee Meeting, Destin, FL, 2002.
42. Van Wie, D.M.; Thompson, M.W.; D'Alessio, S.M.; and Grossman, K.R.: Refurbishment of the JHU/APL Hypersonic Airbreathing Engine Test Facilities. AIAA Paper 2000–2645, 2000.
43. Rice, T.; and Smith, T.D.: Modes 1 and 4 Testing of an Axisymmetric GTX RBCC Engine. Proceedings of the JANNAF 26th Airbreathing Propulsion Subcommittee Meeting, Destin, FL, 2002.
44. NASTRAN user's Manual. NASA–SP–222, 1986.
45. Jarmon, D.C.; Warburton, B.; Briggs, V.; Freedman, M.R.; and Barnett, T.: GTX Propulsion Materials Verification. Proceedings of the JANNAF 26th Airbreathing Propulsion Subcommittee Meeting, Destin, FL, 2002.
46. Warburton, B.; Jaskowiak, M.: GTX Heat-Exchanger Technology Verification. Proceedings of the JANNAF 26th Airbreathing Propulsion Subcommittee Meeting, Destin, FL, 2002.

Table 1.—GTX reference vehicle characteristics

Propulsion	
Thruster chamber pressure range	400 to 2000 psia
Thruster O/F	7
Thruster throat area	0.00682 A <sub>C</sub>
Maximum inlet contraction ratio (A <sub>C</sub> /A <sub>2</sub> )	12
Exit-to-capture area ratio (A <sub>9</sub> /A <sub>C</sub> )	2.503
Orbit and Trajectory Constraints	
220 nmi/28.5° easterly	
Maximum dynamic pressure	1500 psfa
Maximum air-breathing duct pressure	10 atm
Maximum total acceleration	4 g
Angle-of-attack range	± 6°
Performance	
Equivalent, effective specific impulse, I*	503 sec
Total ΔV	25,141 ft/sec
Initial-to-final mass ratio	4.38
Lift-off thrust-to-weight ratio	1.8

Table 2.—Reference vehicle weight summary

Assembly name	Weight (lbs)		Comment
	Subassembly	Total	
Fuselage		11,620	
Aero-shell	5675		C/SiC sandwich panels
Aero-shell sub-structure	5389		C/C construction
Thermal protection	556		Saffil® high temperature insulation
Propellant tanks		6208	
LH <sub>2</sub> tank + insulation	4737		10,567 ft <sup>3</sup>
LOX tank + insulation	1062		1946 ft <sup>3</sup>
Tank adapter	322		PMC construction
Payload adapter	87		PMC construction
Wings and tail		2992	C/C structure, C/SiC sandwich panel skin
Propulsion		14,847	See figure 6
Dorsal	4813		Tail has lighter loads
Port	5017		
Starboard	5017		
Landing gear		1997	Sized for dry weight
Nose	450		
Main	1547		
Equipment		3936	Electrical, hydraulic, propellant feed, etc.
LOX propellant		145,970	LN <sub>2</sub> temperature O <sub>2</sub>
Ascent	138,182		
Other	7788		De-orbit, boil-off, residuals, and margin
LH <sub>2</sub> propellant		50,720	Densified
Ascent	48,487		
Other	2233		De-orbit, boil-off, residuals, and margin
Total dry weight		51,621	Includes "other" propellants
Payload		300	
GLOW		238,590	

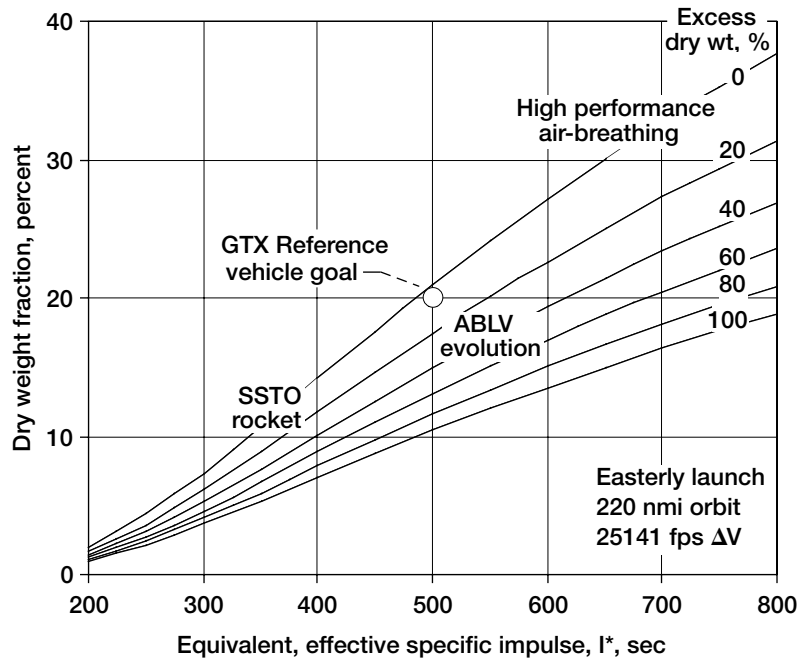


Figure 1.—Air-breathing launch vehicle (ABLV) system performance comparisons.

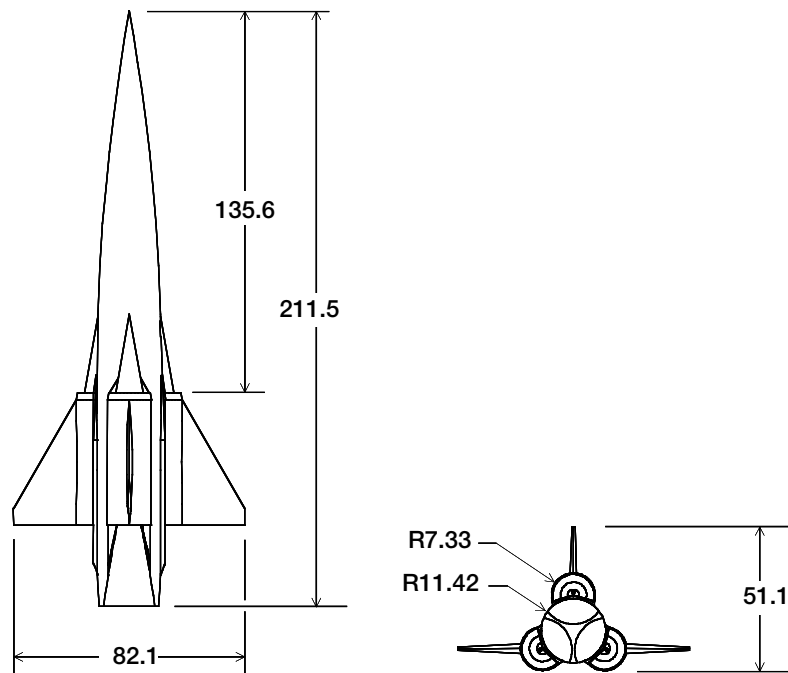


Figure 2.—GTX reference vehicle configuration (dimensions in feet).

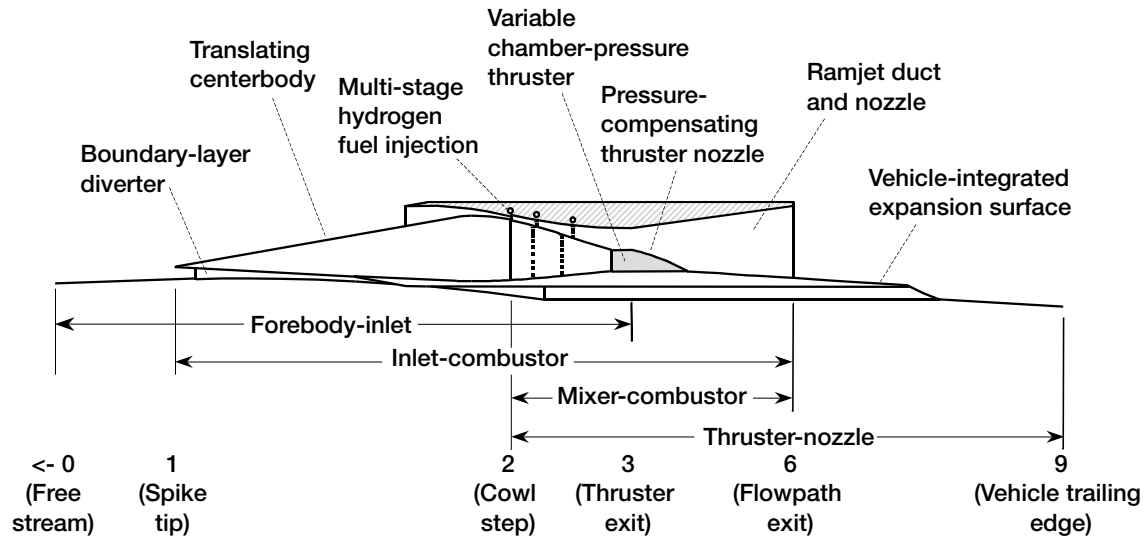
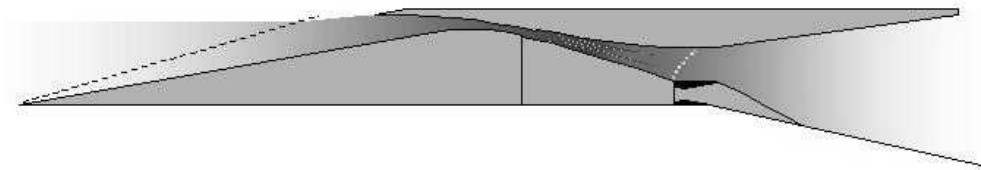


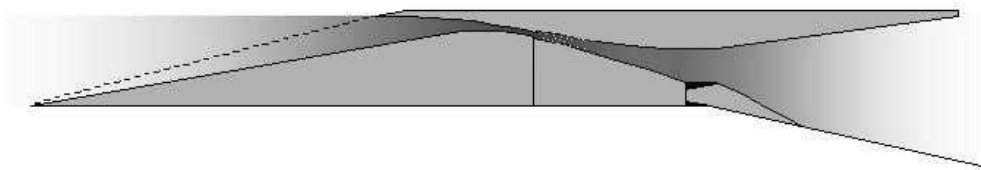
Figure 3.—Flow path cut-away showing key components and station designations.



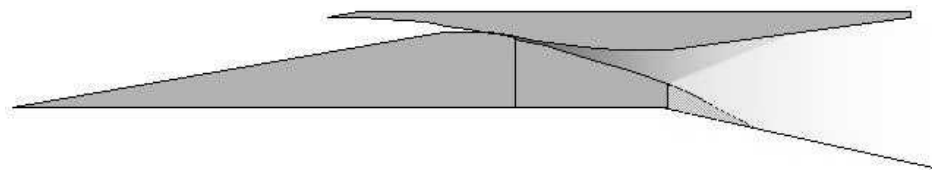
(a) Mode I—Rocket/ramjet combined-cycle, lift-off to Mach 2.5.



(b) Mode II—Thermally-choked ramjet, Mach 2.5 to Mach 5.5.



(c) Mode III—Scramjet, Mach 5.5 to Mach 11.



(d) Mode IV—Rocket Mach 11 to orbit, circularization.

Figure 4.—GTX reference vehicle ascent propulsion modes.

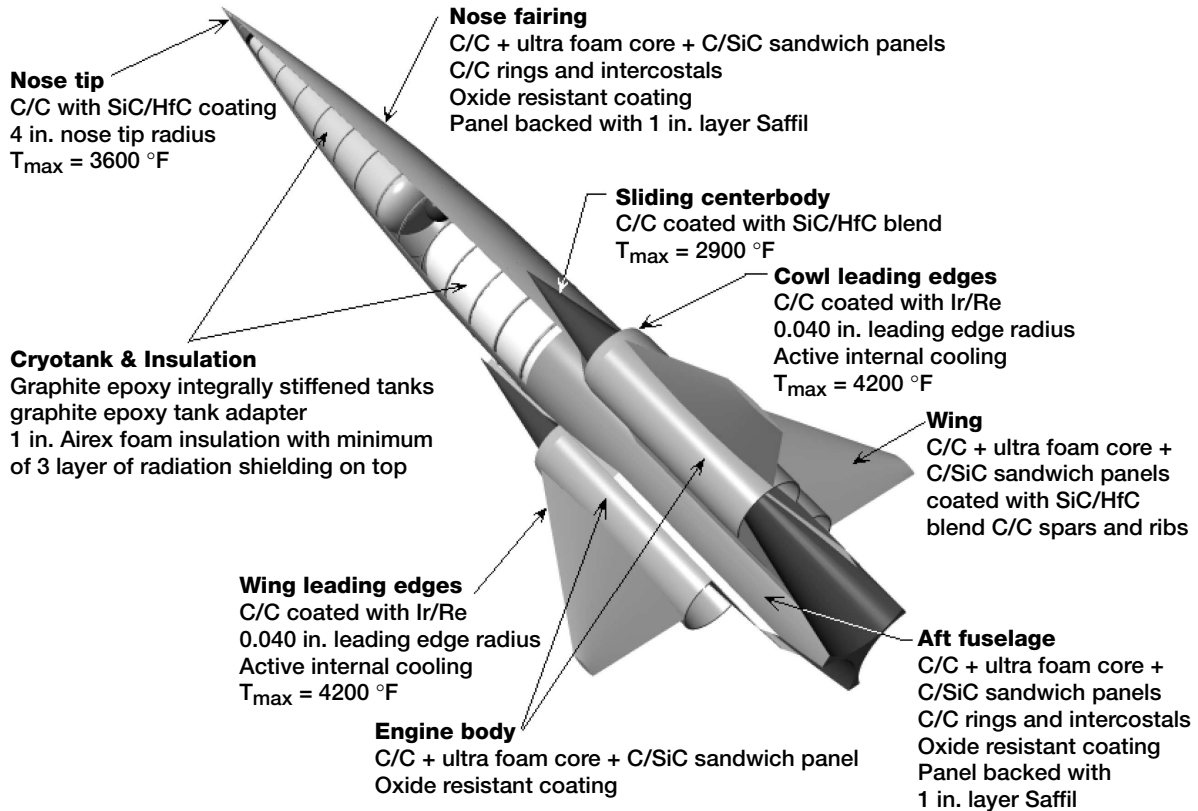


Figure 5.—Vehicle cut-away showing major structural elements and materials.

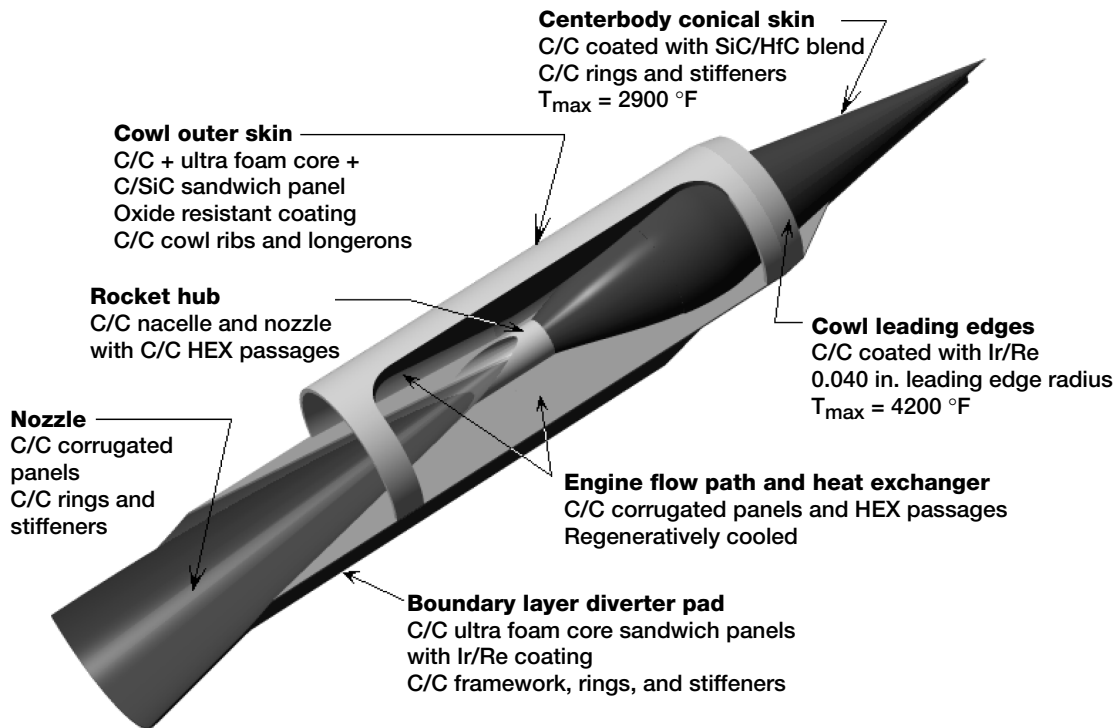


Figure 6.—Propulsion system cut-away showing major structural elements and materials.

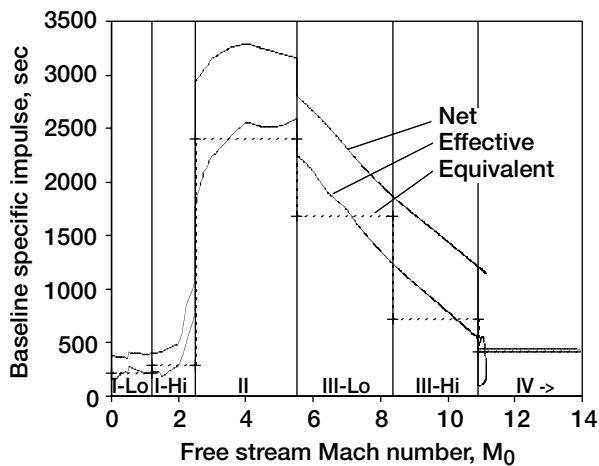


Figure 7.—Reference vehicle performance and trajectory segments used for sensitivity analysis.

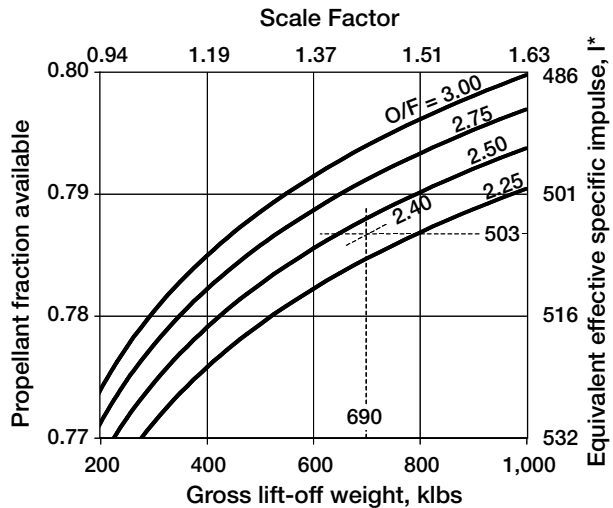


Figure 9.—Sensitivity of GLOW to  $I^*$  for various vehicle O/F.

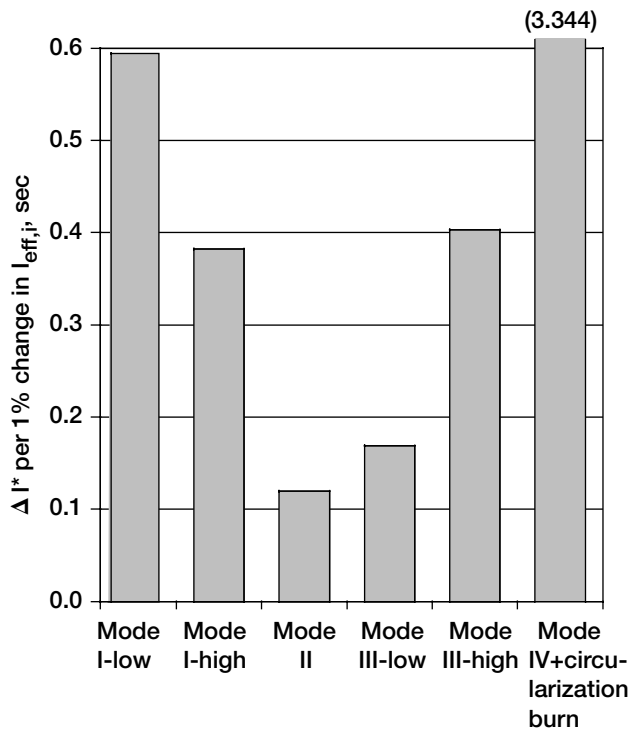


Figure 8.—Sensitivity of  $I^*$  to a 1% change in  $I_{eff}$ .

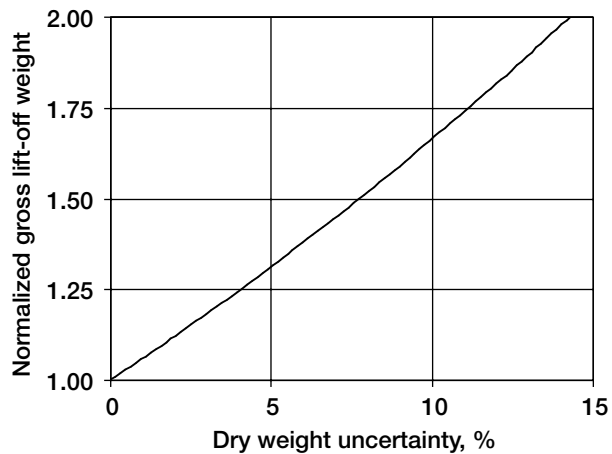
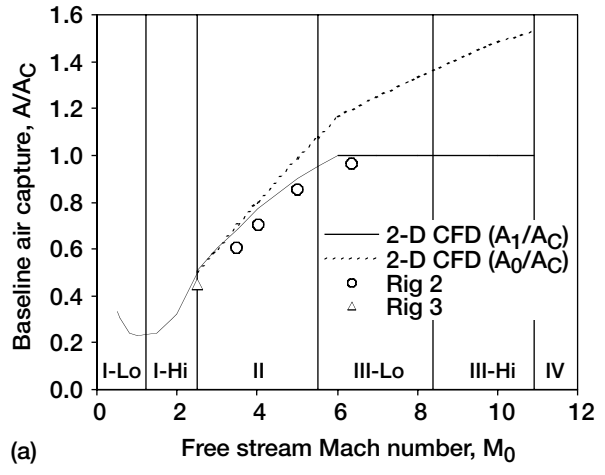


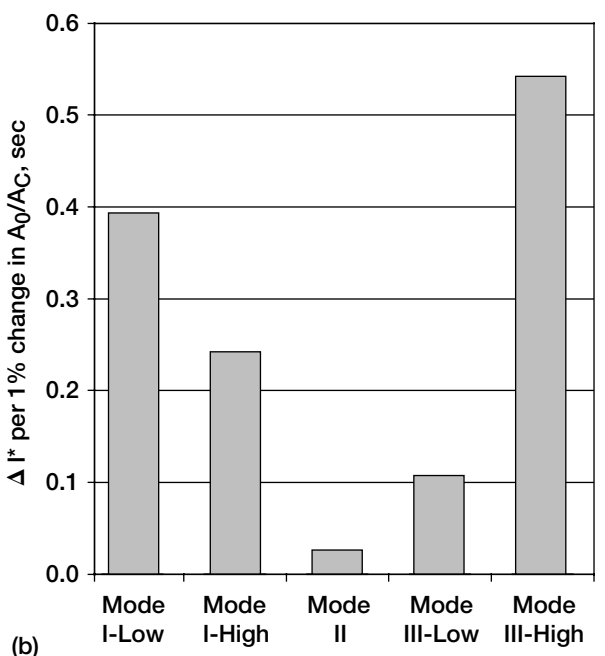
Figure 10.—Sensitivity of GLOW to dry weight uncertainty.

Propulsion Mode	Forebody-inlet	Inlet-combustor	Mixer-combustor	Thruster	Thruster-nozzle
I-Lo (Ram/Rocket)	n/a	n/a	1	6	8
I-Hi (Ram/Rocket)	3	3	1	6	8
II (Ramjet)	3	2, 3, 4	1		8
III-Lo (Scramjet)		2, 4, 9	n/a		8
III-Hi (Scramjet)		4, 9	n/a		8
IV (Rocket)				6	7, 8

Figure 11.—Matrix of component development and validation rigs.

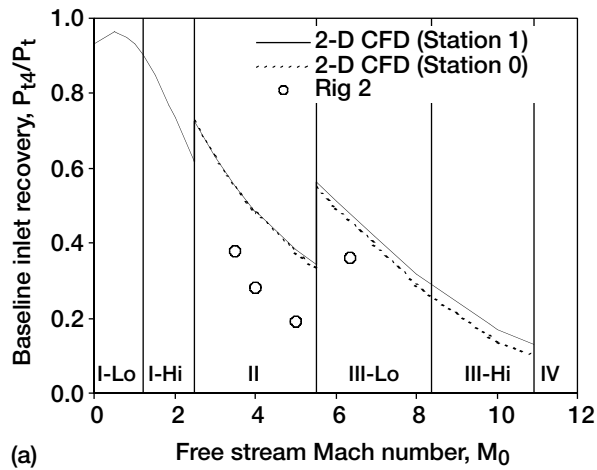


(a)

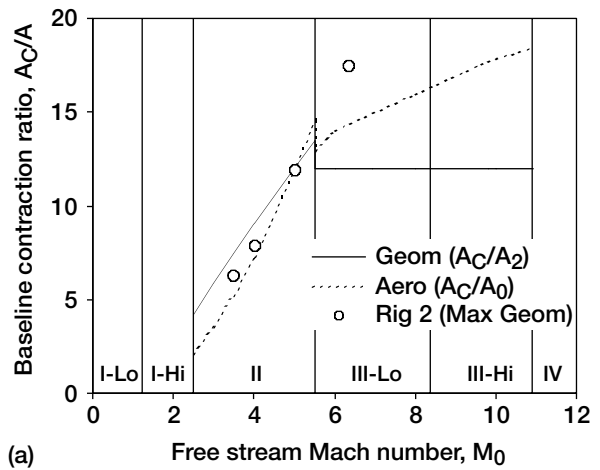


(b)

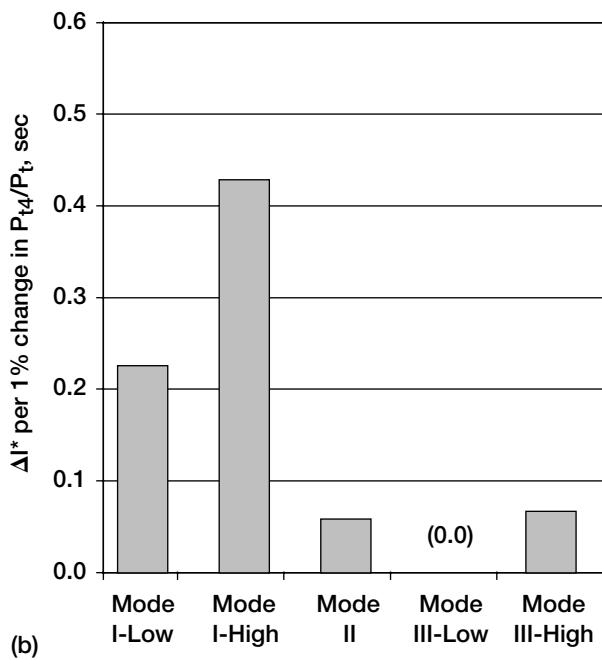
Figure 12.—Reference vehicle air capture. (a) Air capture ratio at free stream and station 1 showing the effect of forebody compression. (b) Sensitivity of  $I^*$  to a 1% change in air capture.



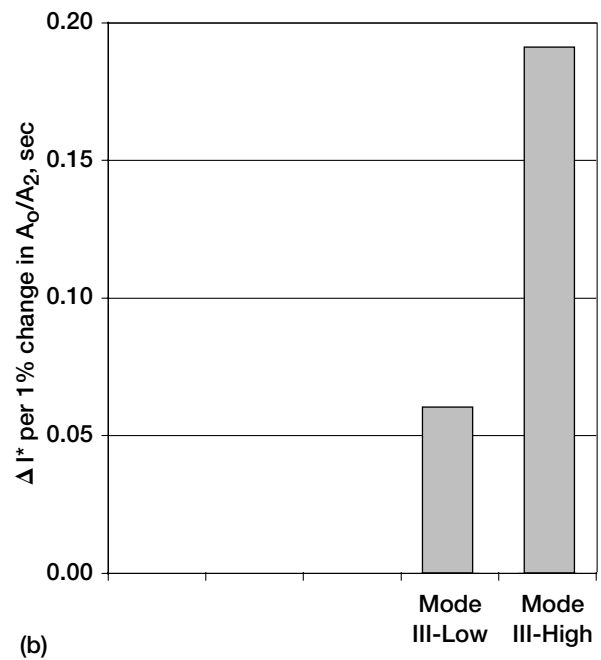
(a)



(a)



(b)



(b)

Figure 13.—Reference vehicle inlet recovery.  
 (a) Baseline inlet recovery based on free stream and station 1 total pressure. (b) Sensitivity of  $I^*$  to a 1% change in inlet recovery.

Figure 14.—Reference vehicle inlet contraction ratio.  
 (a) Baseline geometric and aerodynamic contraction ratios. (b) Sensitivity of  $I^*$  to a 1% change in inlet contraction ratio.

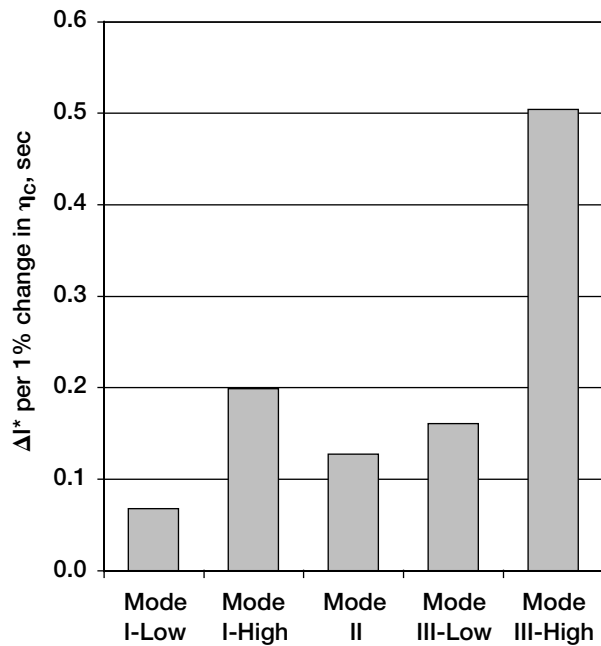
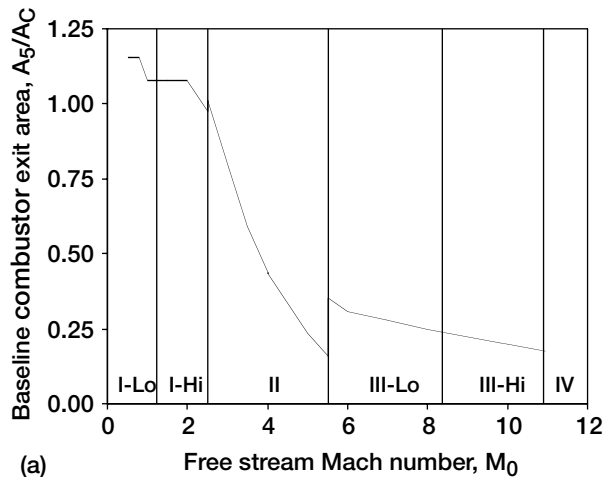


Figure 15.—Sensitivity of  $I^*$  to a 1% change in combustion efficiency.



(a)

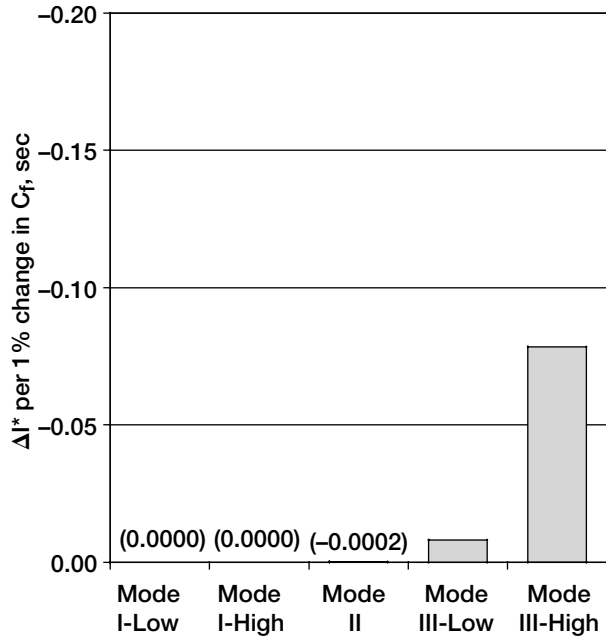
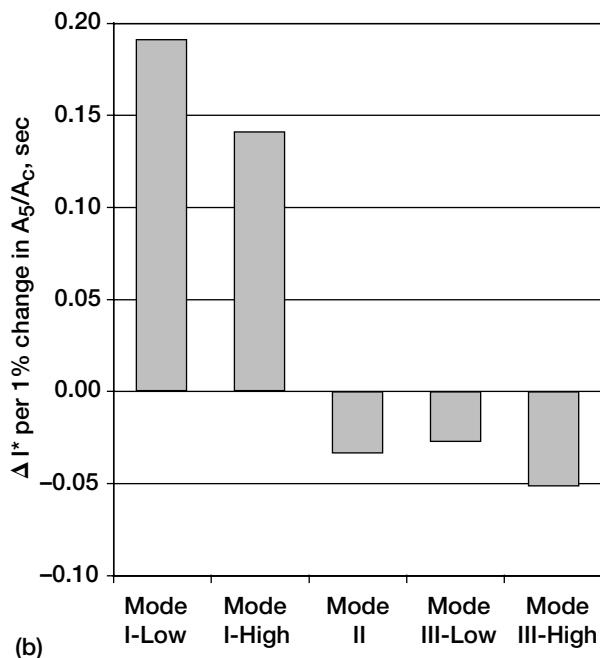


Figure 16.—Sensitivity of  $I^*$  to a 1% change in combustor friction coefficient.



(b)

Figure 17.—Reference vehicle combustor exit area. (a) Baseline combustor exit area. (b) Sensitivity of  $I^*$  to a 1% change in combustor exit area.

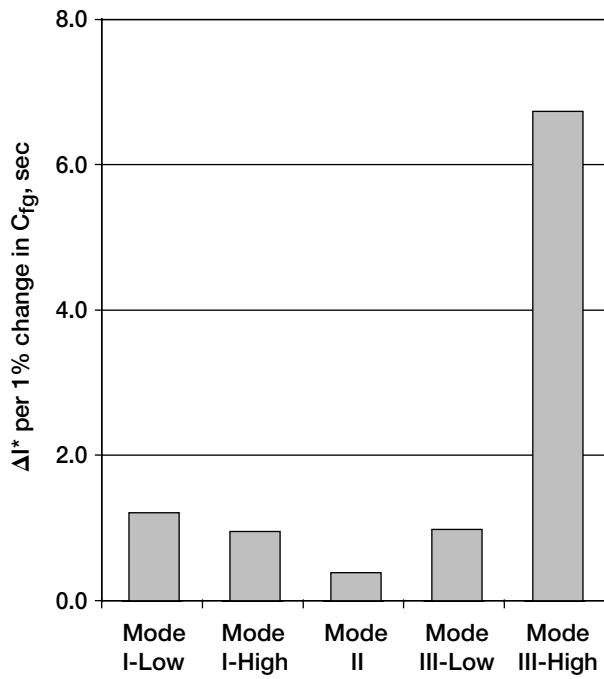
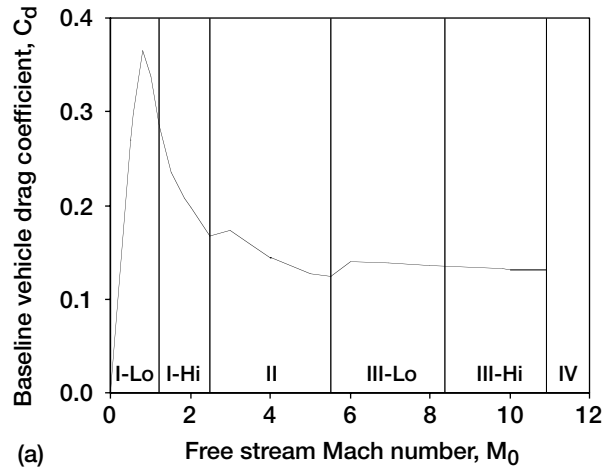
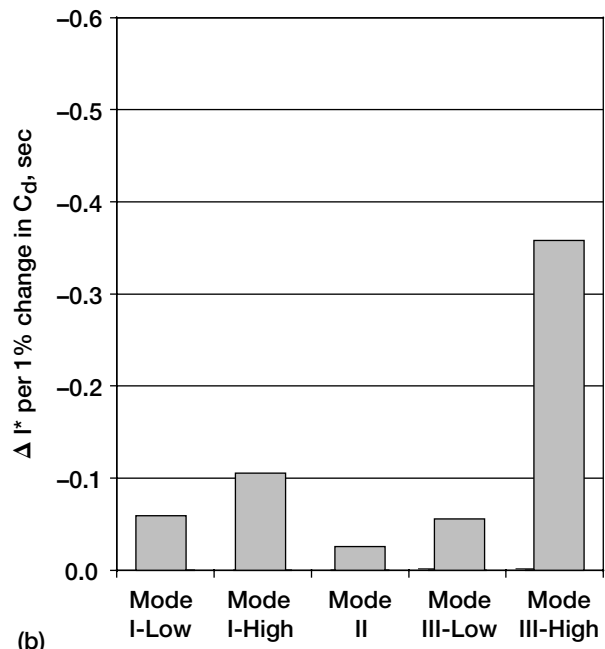


Figure 18.—Sensitivity of  $I^*$  to a 1% change in nozzle gross thrust coefficient.



(a)



(b)

Figure 19.—Reference vehicle drag coefficient. (a) drag coefficient on optimal trajectory. (b) Sensitivity of  $I^*$  to a 1% change in drag coefficient.

<b>REPORT DOCUMENTATION PAGE</b>			<i>Form Approved</i> <i>OMB No. 0704-0188</i>	
Public reporting burden for this collection of information is estimated to average 1 hour per response, including the time for reviewing instructions, searching existing data sources, gathering and maintaining the data needed, and completing and reviewing the collection of information. Send comments regarding this burden estimate or any other aspect of this collection of information, including suggestions for reducing this burden, to Washington Headquarters Services, Directorate for Information Operations and Reports, 1215 Jefferson Davis Highway, Suite 1204, Arlington, VA 22202-4302, and to the Office of Management and Budget, Paperwork Reduction Project (0704-0188), Washington, DC 20503.				
<b>1. AGENCY USE ONLY (Leave blank)</b>		<b>2. REPORT DATE</b> April 2002	<b>3. REPORT TYPE AND DATES COVERED</b> Technical Memorandum	
<b>4. TITLE AND SUBTITLE</b>  Performance Validation Approach for the GTX Air-Breathing Launch Vehicle			<b>5. FUNDING NUMBERS</b>  WU-708-90-63-00	
<b>6. AUTHOR(S)</b>  Charles J. Trefny and Joseph M. Roche				
<b>7. PERFORMING ORGANIZATION NAME(S) AND ADDRESS(ES)</b>  National Aeronautics and Space Administration John H. Glenn Research Center at Lewis Field Cleveland, Ohio 44135-3191			<b>8. PERFORMING ORGANIZATION REPORT NUMBER</b>  E-13263	
<b>9. SPONSORING/MONITORING AGENCY NAME(S) AND ADDRESS(ES)</b>  National Aeronautics and Space Administration Washington, DC 20546-0001			<b>10. SPONSORING/MONITORING AGENCY REPORT NUMBER</b>  NASA TM-2002-211495	
<b>11. SUPPLEMENTARY NOTES</b>  Prepared for the Combustion, Airbreathing Propulsion, Propulsion Systems Hazards, and Modelling and Simulation Subcommittees Joint Meeting sponsored by the Joint Army-Navy-NASA-Air Force, Destin, Florida, April 8-12, 2002. Responsible person, Charles J. Trefny, organization code 5880, 216-433-2162.				
<b>12a. DISTRIBUTION/AVAILABILITY STATEMENT</b>  Unclassified - Unlimited Subject Categories: 15, 20, and 39 Available electronically at <a href="http://gltrs.grc.nasa.gov/GLTRS">http://gltrs.grc.nasa.gov/GLTRS</a> This publication is available from the NASA Center for AeroSpace Information, 301-621-0390.			<b>12b. DISTRIBUTION CODE</b>	
<b>13. ABSTRACT (Maximum 200 words)</b>  The primary objective of the GTX effort is to determine whether or not air-breathing propulsion can enable a launch vehicle to achieve orbit in a single stage. Structural weight, vehicle aerodynamics, and propulsion performance must be accurately known over the entire flight trajectory in order to make a credible assessment. Structural, aerodynamic, and propulsion parameters are strongly interdependent, which necessitates a system approach to design, evaluation, and optimization of a single-stage-to-orbit concept. The GTX reference vehicle serves this purpose, by allowing design, development, and validation of components and subsystems in a system context. The reference vehicle configuration (including propulsion) was carefully chosen so as to provide high potential for structural and volumetric efficiency, and to allow the high specific impulse of air-breathing propulsion cycles to be exploited. Minor evolution of the configuration has occurred as analytical and experimental results have become available. With this development process comes increasing validation of the weight and performance levels used in system performance determination. This paper presents an overview of the GTX reference vehicle and the approach to its performance validation. Subscale test rigs and numerical studies used to develop and validate component performance levels and unit structural weights are outlined. The sensitivity of the equivalent, effective specific impulse to key propulsion component efficiencies is presented. The role of flight demonstration in development and validation is discussed.				
<b>14. SUBJECT TERMS</b>  Single stage to orbit vehicles; Rocket-based combined-cycle engines; Reusable launch vehicles			<b>15. NUMBER OF PAGES</b>  27	
			<b>16. PRICE CODE</b>	
<b>17. SECURITY CLASSIFICATION OF REPORT</b>  Unclassified	<b>18. SECURITY CLASSIFICATION OF THIS PAGE</b>  Unclassified	<b>19. SECURITY CLASSIFICATION OF ABSTRACT</b>  Unclassified	<b>20. LIMITATION OF ABSTRACT</b>	